Journal Pre-proof

Enhanced oxidation and graphitization resistance of polycrystalline diamond sintered with Ti-coated diamond powders

Xiaohua Sha, Wen Yue, Haichao Zhang, Wenbo Qin, Dingshun She, Chengbiao Wang

PII: S1005-0302(20)30031-1

DOI: https://doi.org/10.1016/j.jmst.2020.01.031

Reference: JMST 1898

To appear in: *Journal of Materials Science & Technology*

Please cite this article as: Sha X, Yue W, Zhang H, Qin W, She D, Wang C, Enhanced oxidation and graphitization resistance of polycrystalline diamond sintered with Ti-coated diamond powders, *Journal of Materials Science and amp; Technology* (2020), doi: https://doi.org/10.1016/j.jmst.2020.01.031

Research Article

Enhanced oxidation and graphitization resistance of polycrystalline diamond sintered with Ti-coated diamond powders

Xiaohua Sha [1,4], Wen Yue [1,2,*], Haichao Zhang [1], Wenbo Qin [1], Dingshun She [1,2], Chengbiao Wang [1,3,*]

[1] *School of Engineering and Technology, China University of Geosciences (Beijing), Beijing 100083, China*

[2] *Zhengzhou Institute, China University of Geosciences (Beijing), Zhengzhou 451283, China*

[3] *Zhengzhou Institute of Multipurpose Utilization of Mineral Resources, Chinese Academy of Geological Sciences, Zhengzhou 450006, China*

[4] *Ningxia Vocational Technical College of Industry and Commerce, Ningxia 750021, China*

* Corresponding authors. Prof., Ph.D.; Tel.: +86 10 82321981.

E-mail addresses: cugbyw@163.com (W. Yue); cbwang@cugb.edu.cn (C.B. Wang).

[Received 5 July 2019; Received in revised form 27 September 2019; Accepted 4 October 2019]

To improve the oxidation and graphitization resistances of the polycrystalline diamond (PCD), Ti coating was deposited on the diamond powders via magnetic sputtering method, which achieved a uniform TiC protection barrier in PCD during the sintering process. The phase compositions, microstructures and thermal stability of Ti-PCD were characterized by X-ray diffraction (XRD), Auger electron spectroscopy (AES), scanning electron microscopy (SEM) and thermal gravimetric-differential scanning calorimetry (TG-DSC). The results demonstrate that the oxidation and graphitization resistances of PCD are strengthened due to the existence of TiC phase, which acts as an effective inhibitor. The as-received inhibitor delays the oxidation and graphitization of PCD, elevating their initial temperature by ~50 °C and ~100 °C, respectively. During the annealing treatment of Ti-PCD, the priory oxidation of TiC, which produces TiO_2 as an oxygen barrier, postpones the diamond oxide. Moreover, the TiC barrier also protects diamond grains from direct contact with cobalt, thus a lower cobalt-catalytic graphitization, and yields to an improved graphitization resistance of PCD. The enhanced oxidation and graphitization resistances of PCD are of significant importance for practical applications to elevated temperatures.

Key words: Polycrystalline diamond; Ti-coated diamond powder; TiC barrier; Oxidation resistance; Graphitization resistance

1. Introduction

Since the early 1970s, the sintered polycrystalline diamond (PCD) has been utilized to drilling tools. Wentorf et al.[1,2] have exploited a route to infiltrate cobalt (Co) to diamond layer under high temperature and high pressure. Normally, the Co infiltrates to the diamond layer and acts as an agent to form diamond-diamond (D-D) bonds during the sintering process. The Co offers great wetting of diamond crystallites, thus leading to the high hardness of PCD. Because of its excellent mechanical properties, such as high hardness, great thermal conductivity and excellent wear performance, the PCD has been widely applied to the petroleum or geological drilling fields[3-6]. However, the application of PCD is severely limited due to its poor thermal stability, including low oxidation and graphitization resistances, as a consequence of catastrophic loss of the mechanical properties.

Diamond presents thermodynamically metastable state at atmospheric pressure[7,8]. Generally, when the electronic configuration of sp^3 transfers to sp^2, a phase conversion in diamond may take place. For example, diamond might transfer to graphite at high temperatures (>1700 °C)[9,10]. However, transition metals with intermediate reactivity, such as Fe, Ni, Co, and Cr, normally worsen the thermal stability of PCD by a certain degree, namely, they accelerate the graphitization of diamond[11,12]. In this case, the graphitization temperature of PCD has been declined to 700 °C due to the catalysis of Co, which severely limits the lifetime and efficiency of PCD tools at elevated temperatures[13]. Some research has focused on the methods to lower the content of Co in the PCD. In most cases, the electrolysis and chemical treatments are utilized[14,15]. Indeed, these treatments for PCD have been attested to enhance the thermal stability on some degree. Nevertheless, the removal of Co would cause a large amount of pores and thus lead to substantial damage of the strength and toughness of PCD. For these reasons, a protective barrier without any damage to the PCD is imperative when the enlarged usefulness of PCD is especially needed.

In addition, the oxygen susceptibility at elevated temperatures is another inferior feature of PCD. The oxidation of diamond typically begins at approximately 700 °C when annealed in oxidative atmospheres[16,17]. The PCD tools are also subject to be oxidized at similar temperatures (above ~750 °C) under oxidizing conditions[18]. Normally, the gaseous product of the oxidation of diamond immediately escapes to environments and leads to a large amount of oxygen corrosion pits, thus causing the deteriorated mechanical properties of PCD. Hence, how to enhance the oxidation resistance of diamond has been explored for decades for the purpose of applying diamond to oxygen-containing environments[19-22]. Thanks to the development of oxygen barrier for diamond, in particular the protective coating on diamond surface, which can inhibit direct oxygen corrosion[23-28]. Coating boron carbide on the diamond is also demonstrated as an efficient route for improving the oxidation resistance of diamond[23]. It is reported that the B_2O_3 phase would be priorly formed and act as an oxygen barrier layer when heated in air. The titanium (Ti) coating was deposited in Ref. [24] to increase the oxidation temperature of diamond grits to 1024 °C. Zuo et al. found that the wheels made from nickel-coated diamond powders processed excellent wear resistance[25]. In addition, an enhanced inoxidizability of PCD was achieved by sintering Si-coated diamond powders[26]. Therefore, coating film on the diamond powders can

efficiently impede oxygen corrosion of PCD at high temperature.

Based on the above studies, a coating deposited on the diamond powders would be of great significance to the oxidation and graphitization resistances of PCD. The coating not only acts as an oxygen barrier to inhibit oxidation corrosion of PCD, but also prevents the PCD from cobalt-catalytic graphitization by hindering the direct contact between cobalt and diamond grains.

In the present work, a PCD was produced by sintering Ti-coated diamond powders. The phase compositions, microstructures and thermal stability of the Ti-PCD were studied, while the contribution of the Ti coating to the oxidation and graphitization resistances enhancement of Ti-PCD was systematically investigated.

2. Materials and methods

2.1. Materials synthesis

The raw materials for preparing Ti-coated diamond powders are commercial product (Zhongnan Diamond Co., Ltd.). A Ti coating on the diamond powders was deposited via magnetron sputtering (Beijing Technol Science Co., Ltd.) using a pure Ti target (99.99%) at a pressure of 0.4 Pa. The distance between the magnetrons and substrate holder was 20 cm. In addition, the substrate holder was vibrated ultrasonically during the whole sputtering process to make the diamond powders rolled continuously and obtain an even-covered Ti coating. A high-voltage and Ar gas (99.99%) were introduced to the working chamber to produce sputtering ion beam at arranged base pressure (5×10^{-3} Pa). To clean the deposition surface, the Ar^+ ion beam was used to sputter the diamond powders for 20 min before deposition. The sputtering power and discharging current for the Ti target were kept constant at 150 W and 0.5 A, respectively. The deposition was performed at 25 °C. Prior to the deposition, the powders were firstly boiled in HNO_3 and NaOH solution successively, and then annealed in vacuum (P=10^{-3} Pa) at 200 °C for 24 h to obtain a clean surface without a large amount of absorbed substance.

The polycrystalline diamond compact (PDC) was synthesized at Zhongnan Diamond Co., Ltd. The PCD layer is placed on the WC-Co substrate (WC-16 wt% Co). The diameter and thickness of the PDC are 45.0 mm and 2.9 mm, respectively. The PCD layer is as thick as 0.53 mm, while that of WC-Co substrate is 2.37 mm. In addition, the test sample synthesized with uncoated diamond powders is named P-PCD and that synthesized with Ti-coated diamond powders is named Ti-PCD.

2.2. Annealing tests

To examine the thermal behaviours of the Ti-PCD, the samples were annealed at room temperature (RT), 700, 750, 800, 850 and 900 °C for 30 min in air with a muffle furnace (SX-8-10). The annealing temperature was measured by a thermocouple (± 20 °C). The samples were ultrasonically rinsed with acetone for 30 min

and then dried by nitrogen blower before annealing treatment. When the samples were annealed, the temperature increased by a rate of ~20 °C/min. Then, an air-cooling of the samples treated after annealing tests was carried out. As for the choosing of the annealing temperatures, we selected them on the base of our previous work[18,29]. For the P-PCD samples, the diamond phase transferred to graphite at 700 °C, while the oxidation of diamond occurred at the temperatures above 750 °C. The same annealing temperatures were selected to detect the changes of oxidation and graphitization resistances between Ti-PCD and P-PCD samples.

2.3. Characterization methods

The scanning electron microscope (SEM; CS3400) was utilized to study the surface topographies of Ti-coated diamond powders and Ti-PCD samples. The chemical compositions were analysed by the energy dispersive X-ray spectroscopy (EDS; Oxford EDX-450). Prior to the SEM analysis, the samples were treated by spray-platinum due to the weak electrical conductivity of the Ti-PCD. A PHI-700 Auger electron spectroscopy (AES) was used to measure the thickness of Ti coating deposited on diamond powders. The thickness of Ti coating is inferred based on the sputtering time, which is calibrated by sputtering the SiO_2 film. The particle size of the Ti-coated diamond powders was measured by the Fisher sub-sieve sizer. The thermal gravimetric-differential scanning calorimetry (TG-DSC) was performed with a heating rate of 20 °C /min from 20 °C to 1200 °C (STA449F3, German). An air atmosphere was flowed through the chamber during the measurement. The D/max-2550X X-ray diffraction (XRD) (CuK_α: 40 kV, 200 mA) was conducted to investigate the phase structures of Ti-coated diamond powders and annealed Ti-PCD. The compositions of the annealed Ti-PCD were determined by a LabRAM HR Evolution Raman spectrometer with a 514.5 nm wavelength of the Ar+ laser. The NanoMap-D 3D surface profilometer was utilized to measure surface topographies of the annealed Ti-PCD. An Atomic Force Microscope-Lateral Force (AFM-LF) (MFP-3D) was employed to measure the surface topography of the Ti-PCD surfaces. The point probe plus contact mode probe with a Si_3N_4 tip was selected. The scanning frequency was 1 Hz and the scanning scope was 20 μm×20 μm. Prior to the above-mentioned analyses, the annealed samples were ultrasonically rinsed with acetone for 30 min and then dried by nitrogen blower.

To study the wear properties of PCD samples, the wear tests were conducted by a CSM-TRN ball-on-disc tribometer (relative humidity, 35% ± 3%). A Si_3N_4 ball with a diameter of 6 mm was used as a mating ball, while the PCD was used as a disk. During the tests, the Si_3N_4 ball was fixed and the PCD disc was rotated with a frequency of 400 r/min and a turning radius of 2.5 mm, corresponding to a liner sliding velocity of ~105 mm/s. The wear test lasted 30 min with a normal load of 20 N. Each test in the experimental conditions was repeated three times. The NanoMap-D 3D surface profilometer was utilized to measure the surface topography of the worn P-PCD and Ti-PCD. The wear rate of the PCD samples was calculated by the Archard wear

equation:

$$V = k \times F \times s \quad (1)$$

where V (mm^3) is the wear volume of samples, obtained from the cross-sectional area of the wear track measured by the NanoMap-D 3D surface profilometer, F (N) is the normal load, s (mm) is the sliding distance, and k is the wear rate per unit load and per unit distance. Five detecting positions were selected at random on the wear track of the PCD discs, and an average value of the cross-sectional area was calculated.

3. Results

3.1. General characterization of the materials

To improve the thermal stability of PCD, a Ti coating was deposited on the diamond powders. Fig. 1 shows the morphology and phase composition of the Ti-coated diamond powders. The Ti-coated diamond powders present anomalous shapes with sharp edges and cleavage steps, which is resulted from the mechanical milling (Fig. 1(a)). Moreover, the obtained Ti coating presents a continuous and compact structure without any cracks, spreading on the surfaces of the diamond powders uniformly (Fig. 1(b) and (c)). Fig. 1(d) reveals the XRD pattern of the Ti-coated diamond powders. The three main peaks at 2θ= 35.1°, 38.1° and 40.0° correspond to (100), (002) and (101) crystal planes of a titanium phase (α-Ti), respectively, suggesting the successful deposition of Ti coating. This verifies the EDS mapping results. The thickness of the Ti coating is calculated from the sputtering time of AES. As seen in Fig. 1(e), the elemental depth profile of Ti-coated diamond powders can be divided into three zones based on the distributions of Ti and C along depth. The first zone is from the sample surface to a depth of ~500 nm (corresponding to a sputtering time of 0-35 min), where the Ti content keeps a stable value of ~80%. The second zone is from a depth of ~500 nm to ~950 nm (corresponding to a sputtering time of 35 min-65 min). This zone reveals a thin transition layer, where the Ti content decreases simultaneously, while C content increases. This suggests that the C in the diamond powder diffuses towards the Ti coating during processing. The third zone presents a depth > 950 nm (corresponding to a sputtering time > 65 min). This zone reveals a C content of almost 100% and the Ti can hardly be detected, which features the diamond powder substrate. It is identified that the first zone is entirely composed of Ti coating with a thickness of ~500 nm, which is directly coated on the diamond powder surface. The particle size distribution of the as-received Ti-coated diamond powders is narrow (Fig. 1(f)) with designated average powder diameter (D_{50}) of 23.75 μm.

Fig. 2 presents the morphologies and phase compositions of the Ti-PCD. As shown in Fig. 2(a), the surface roughness average (Ra) of Ti-PCD reaches a value of ~3 nm. In comparison to the typical micrograph of the Ti-PCD surface and its corresponding EDS maps in Fig. 2(b)-(e), it can be observed in that the Ti and Co elements distribute along the boundaries of diamond grains. The D-D bonds can be observed at the interfaces of

the diamond grains, which demonstrate that excellent bonding among diamond grains was achieved for the Ti-PCD after the sintering process. The bonding guarantees that the PCD process excellent physical and mechanical properties[23,30]. In addition, some tiny holes distribute along the boundaries of the diamond grains, which is formed during the sintering process due to the exfoliation of the fine diamond powders. To understand the phase structure of the Ti-PCD, the XRD was performed. It is presented in Fig. 2(g) that three new peaks located at 2θ= 35.9°, 41.8° and 60.7° correspond to (111), (200) and (220) crystal planes of a titanium carbide (TiC) phase, respectively, which replace those of Ti phase for Ti-coated diamond powders. This phenomenon indicates that the Ti coating deposited on diamond powders has interacted with diamond and formed a TiC phase during the sintering processing.

3.2. Thermal damage behaviours

The thermal stability of the diamond composites strongly relies on the diamond types, synthesis methods and catalysts. The thermoanalytical study of diamond powders and PCD with TG-DSC is given in Fig. 3. For the uncoated diamond powders, a weight loss of ~1 wt% occurs from 20 °C to ~600 °C, which is attributed to the release of absorbed gases or moisture on the surfaces of diamond powders. Moreover, when the temperature increases from approximately 664 °C, the mass curve shows an abrupt decreasing trend, accompanying by a strong oxidized exothermal peak in DSC curve. This indicates that the uncoated diamond powder begins to oxidize at this temperature, and the gaseous products leads to substantial mass loss. For the Ti-coated diamond powders, as seen in Fig. 3(b), it reveals a stronger oxidized exothermal peak of diamond at ~725 °C, which is ~50 °C higher than that of the uncoated diamond powders. In addition, note that a small quantity of weight gain accompanied by a stronger exothermal peak was observed in the temperature range of ~200 °C to ~725 °C, which might be due to the oxidation of Ti coating. Therefore, it can be confirmed that the oxidation of Ti coating occurs prior to that of the diamond powder. When heated in oxygen-containing environment, the Ti coating on the Ti-coated diamond powders contacts with oxygen and leads to an anterior oxidation. Then, the interior diamond powder begins to be oxidized after that of the Ti coating. Namely, the Ti coating acts as an oxygen barrier to prevent immediate oxidation of diamond powders during annealing treatment, hence yields to an improved oxidation resistance of Ti-coated diamond powders.

The TG-DSC curves for PCD samples are presented in Fig. 3(c) and (d). To exclude the interference of the WC-Co substrate, the cemented carbide substrate was mechanically removed before the tests. The TG-DSC results for PCD samples display similar curves to those of the diamond powders. A slight exothermal peak due to the absorbate release appears from ~200 °C to ~810 °C for the P-PCD, while that of the Ti-PCD postpones to ~868 °C with a stronger intensity. After then, tremendous weight loss attributed to the oxidation of diamond can be observed. As a whole, the initial oxidizing temperature Ti-PCD is ~50 °C higher than that of the P-PCD.

Supposedly, this delayed oxidation of Ti-PCD may be attributed to the fact that the TiC could be oxidized and form TiO_2 in this temperature range. In addition, the uncoated diamond powder (664 °C) and the Ti-coated diamond powder (725 °C) have a much lower onset temperature of mass loss compared to the respective sintered compacts, of which P-PCD (810 °C) and Ti-PCD (868 °C). This points to the fact that the diamond powders have more surface area available for oxidation than the PCD. on the DSC curves of P-PCD and Ti-PCD, the endothermal peaks at ~904 and ~1010 °C, respectively, may be result from the chemical decomposition of Co_3O_4[18,30].

Fig. 4 shows the XRD patterns obtained from the Ti-PCD samples annealed at different temperatures. The pattern of the Ti-PCD annealed at 700 °C is almost the same as that of the pristine Ti-PCD (RT Ti-PCD), which suggests that no obvious chemical reaction occurs when the samples were annealed at 700 °C. In addition, it is notably that no visible new phase is found within the limits of instrument on the Ti-PCD surface annealed at 750 °C, but a slight rutile-TiO_2 peak. The appearance of TiO_2 signal must be attributed to the oxidation of TiC at this temperature. This indicates that the TiC begins to oxidize at ~750 °C, which brings into correspondence with the TG-DSC results. Generally, with the increase of annealing temperature, the TiC would interact with adsorbed and residual oxygen in the preform at the temperature of 750 °C[31]:

$$TiC + 2O_2 \rightarrow TiO_2 + CO_2 \quad (2)$$

Moreover, it also can be seen from the XRD patterns that the TiC peaks have completely disappeared at 750 °C, which is a further proof to justify the phase transition from TiC to TiO_2. Therefore, it can be confirmed that the TiC, which was generated by the reaction of the Ti coating and diamond powders during sintering process, transfers to TiO_2 phase by the oxide action at 750 °C annealing treatment in air.

In addition, a substantial phase transformation occurs at the annealing temperatures above 800 °C. A large amount of cobalt oxide (Co_3O_4 and CoO) and a litter amorphous carbon, graphite and TiO_2 are found at 800, 850 and 900 °C. The new cobalt oxide phases are observed with the disappearance of ε-cobalt at the temperatures ranging from 800 °C to 900 °C. Moreover, when the annealing temperature increases to a higher value, the intensity of cobalt oxide phases intensifies. This suggests the gradually reinforced occurrence of cobalt oxidation at this temperature range. The reaction equations are as follows:

$$3Co + 2O_2 \rightarrow Co_3O_4 \quad (3)$$

$$2Co_3O_4 \rightarrow 6CoO + O_2 \quad (4)$$

Moreover, the appearance of graphite peaks demonstrates that the graphitization of Ti-PCD occurs at 800 °C. The graphite peaks tended stronger with the degradation of diamond peaks when the samples were annealed at higher temperatures, which indicates that a much severer graphitization of Ti-PCD takes place at elevated annealing treatment. Our previous work[18] has reported that some graphite phase appeared on the P-PCD surface annealed at 700 °C. Notably, the initial graphitization temperature of Ti-PCD is ~100 °C higher than that of the P-PCD. This indicates that an enhanced graphitization resistance of PCD has been achieved in this work,

which would be of great benefit to the service life of PCD drilling bits. In addition, the degradation of diamond peak mainly comes from the oxidation of diamond phase. Gaseous products are demonstrated to be generated due to the diamond oxidation, which leads to the substantial thermal loss of the Ti-PCD[30]. Moreover, the TiC peak almost completely fades away at the temperature ranging from 800 °C to 900 °C, accompanying by the appearance of TiO_2 peak. According to the above SEM results that the oxidation of TiC has been observed at 750 °C and the TG-DSC results, it can be verified that the TiC is oxidized priorly to the diamond, which occurs at approximately 800 °C. In this case, the oxidation of TiC postpones the diamond oxide during the annealing treatment and thus improves the oxidation resistance of Ti-PCD.

The Raman spectroscopy was carried out to study the chemical characteristics of annealed Ti-PCD surface. As shown in Fig. 5, it presents only a sharp diamond peak (~1334 cm^{-1}) at the annealing temperatures of RT, 700 °C and 750 °C, which infers that the Ti-PCD surface annealed at these temperatures is composed of diamond grains with high purity[18]. For the high temperatures above 800 °C, a broad G peak[32] centred at ~1580 cm^{-1} appears. The G peak demonstrates that the diamond grains begin to graphitize[33,34]. This result confirms that the Ti-PCD begins to graphitize at ~800 °C in air, which increases by ~100 °C to that of the P-PCD. In a word, the Ti-PCD possesses a better graphitization resistance than the P-PCD in air.

As presented in Fig. 6, the SEM morphology features of annealed Ti-PCD surfaces strongly depend on the annealing temperature, especially at high temperatures. Fig. 6(b) and (c) reveal no much visible variation for the Ti-PCD surfaces annealed at 700 °C and 750 °C compared to that of the original sample (Fig. 6(a)), demonstrating that no much chemical reaction occurs at these temperatures. In addition, some spalling pits, which are bigger than the tiny holes of the original Ti-PCD surface, distribute along the diamond boundaries. An acceptable explanation is related to the exfoliation of tiny intergranular diamond grains and the mismatch of thermal expansion coefficients among the diamond, TiC and Co phases[29]. An enlarged SEM image for the Ti-PCD surface annealed at 750 °C is presented in Fig. 7. Notably, a large number of microcracks can be observed around the spalling pits, some of which propagate and converge. For the Ti-PCD, there are some tiny intergranular diamond grains among the original defects of the Ti-PCD surface, and they are inclined to exfoliate when heated, thus yields to the appearance of spalling pits[18]. In addition, the mismatch of thermal expansion coefficients among diamond (3.2×10^{-6} K^{-1}), TiC (7.2×10^{-6} K^{-1}) and cobalt (14.4×10^{-6} K^{-1}) might lead to a high thermal stress and hence induce the formation of microcracks[35,36]. Finally, the further propagation and conversion of the microcracks would result in the exfoliation of fine intergranular diamond grains exfoliate, and thus some spalling pits appear.

When the annealing temperature reaches 800 °C, a very large amount of oxygen corrosion pits distribute along the boundaries of diamond grains without any D-D bonds on the Ti-PCD surface. In addition, the substantial exfoliation of fine diamond grains leads to a large amount of spalling pits. An enlarged SEM image of the thermal surface is revealed in Fig. 8. It can be conducted that some tiny sintering holes, which form

during the synthesis process and distribute along the diamond boundaries, offer substantial contact space for oxygen and induce the oxidation of diamond grains. In this case, the gaseous products of diamond oxidation lead to the formation of imperfections (oxygen corrosion pits) on the Ti-PCD surface. In addition, the XRD result has demonstrated that the cobalt-catalytic graphitization has occurred in the Ti-PCD at high temperatures above 800 °C, which causes cracking and thus exposing more surfaces to for oxidation. This indicates that the cobalt-catalytic graphitization of diamond might indirectly accelerate the oxidation of Ti-PCD. In other words, the cobalt catalyst is substantially harmful to the thermal stability of the PCD. In literatures, the oxygen corrosion of PCD, which results in a large amount of oxygen corrosion pits, always begins at the boundaries of diamond grain and gradually propagates with further oxidation, thus yields to the ruptured D-D bonds and sharply deteriorated mechanical properties of PCD[23,30]. What must be pointed out that the thermal damage morphology of the Ti-PCD surface annealed at 800 °C reveals similar features with that of the P-PCD annealed at 750 °C (seen in our previous work[18]). It confirms that the initial oxidizing temperature of Ti-PCD elevates by ~50 °C than that of the P-PCD. Namely, the Ti coating on diamond powders postpones the oxidation temperature of PCD and improves its oxidation resistance. This phenomenon has also been confirmed by the TG-DSC.

In addition, a much severer oxidation of Ti-PCD occurs at 850 °C (Fig. 6(e)), resulting in the incomplete diamond profile and even oxidized grooves through the diamond grains. Moreover, the cobalt is inclined to interact with oxygen at high temperatures to form CoO and Co_3O_4. According to the EDS maps of the C, Co and O elements, it can be conducted that the extruded phase on the Ti-PCD annealed at 850 °C is mainly composed of Co and O. Fig. 9 further verifies this result. Taking into consideration of the XRD curves of Ti-PCD annealed at 850 °C and the above SEM and EDS results, it is confirmed that some cobalt oxide extruded out from the diamond grains boundaries after annealing treatment. Furthermore, it is notable that the Ti distribution is in great accordance with that of O along the diamond boundaries, implying that the TiC oxides with oxygen and products TiO_2 at this annealing temperature.

With the annealing temperature increases further, the thermal damage morphology tends completely different. Fig. 6(f) shows the morphology features of the Ti-PCD annealed at 900 °C. It is difficult to detect diamond grains but the dendritic structures. Moreover, the EDS mapping results reveal rare C element on the annealed Ti-PCD surface, demonstrating that the diamond has almost been completely oxidized. Instead, a large amount of Co and O uniformly distribute on the detecting surface. It confirms that the dendritic phase is the extruded cobalt oxide. The slight Ti distribution may come from the oxidation of TiC phase. Therefore, when the Ti-PCD is annealed at 900 °C, substantial oxidation occurs, which contains that of the diamond grains, TiC and cobalt phases, thus causing severe oxidized thermal damage.

4. Discussion

The PCD has been demonstrated to be restrictedly applied at elevated temperatures due to the poor thermal stability. Typically, the graphitization temperature of PCD has been declined to 700 °C for the catalysis of cobalt, while the graphitization of the diamond occurs only at high temperatures (>1700 °C)[9,10]. Furthermore, the using of PCD tools in oxygen-containing atmospheres is severely limited due to the extensive oxygen corrosion at temperatures above 750 °C, as a result of the dramatic loss of their mechanical properties[13,17]. Hence, the application of a protection is necessary for the purpose of enlarged usefulness of the PCD to oxidative environments at elevated temperatures.

In this work, the Ti-coated diamond powders were used to enhance the oxidation and graphitization resistances of PCD. The TG-DSC results reveal an obvious enhanced oxidation resistance of Ti-PCD, while the XRD results demonstrate the improved graphitization resistance. Moreover, in combination with the Raman (Fig. 5), SEM (Fig. 6) results and our previous study[18,29], it can be found that the Ti-coated diamond powders delay the oxidation and graphitization of PCD, elevating the initial temperature by ~50 °C and ~100 °C, respectively. Notably, the XRD result for the Ti-PCD sample reveals obvious TiC peak, which replaces that of the Ti phase. Therefore, we can speculate that the as-received TiC phase acts as an effective inhibitor during the annealing treatment.

The above SEM morphologies and corresponding EDS maps demonstrate that the TiC phase distributes along the boundaries of diamond grains. To further verify this result, the chemistry of the interface area has been analysed by EDS line scans. The test surface of Ti-PCD was obtained by the impact treatment. As it given in Fig. 10(a), a diamond grain and spalling pit can be observed on the broken Ti-PCD surface, which might be caused by the inter-granular fracture during the impact treatment. Following the scanning path, a diamond grain is crossed, followed by the interface before entering the spalling pit. The C signal reveals a stable and strong intensity on the diamond grain, while rare Ti signal can be detected. In addition, the interface layer presents a sharply increased signal of Ti, accompanied by the decreased C. Following the interface, the scan enters the spalling pit, where the Ti signal drops to the detection limits, while the C signal abruptly increases to a stable stage. This indicates that the TiC layer forms along the boundaries of diamond grains in the Ti-PCD, which is corresponding to the above SEM results.

In the sintering system of the samples at high temperature and high pressure, pure Ti-coated diamond powders were placed on the tungsten carbide substrate[1,2]. The molten cobalt would act as an agent for forming D-D bonds[37,38]. During sintering process, the molten Co moves by the capillarity through voids among diamond powders[38]. Then, the graphite forms on diamond grain surfaces at high temperature and dissolves into Co liquid phase above the eutectic until saturation[39], and a large recrystallized diamonds precipitates and forms D-D bonds[37]. In this case, the Co plays a crucial role in the physical properties of Ti-PCD. Experiments have shown that carbides can be formed when carbide-forming metal, such as Ti, Zr, V, Cr, is deposited on diamond surfaces and annealed to a sufficiently high temperature[32]. Because the reaction temperature of titanium and

carbon atoms (~400 °C) is far below the melting point of cobalt (~1490 °C), the generation of TiC phase during the sintering process takes place prior to the cobalt meltdown[40,41]. In addition, the generated TiC would not interact with the cobalt. Therefore, an obvious TiC phase can be detected by XRD on the Ti-PCD surface. Both of the TiC and cobalt phases exist in the voids along the diamond margin after sintering process, the former of which encloses to the diamond grains for the lower interfacial energy between strong carbide and diamond. As depicted in Fig. 11, a large amount of D-D bonds exist in the structure, which guarantees the strong bonding strength among diamond grains and thus excellent physical properties of Ti-PCD[23,30]. In addition, the Co and TiC phase fills the voids of diamond grains, while the TiC distributes closely to diamond. Namely, the TiC acts as a barrier in the Ti-PCD and inhibits the direct contact between diamond and cobalt.

In order to determine that whether the TiC barrier worsens the quality of D-D bonding in the Ti-PCD or not, the wear tests were carried out for the Ti-PCD discs annealed at different temperatures. As shown in Fig. 12, the wear rates of the Ti-PCD annealed at different temperatures were compared with those of the P-PCD, which was reported in our previous work[18]. For the pristine PCDs, the wear rate of Ti-PCD (5×10^{-12} mm^3 N^{-1} mm^{-1}) is much lower than that of the P-PCD (22.5×10^{-12} mm^3 N^{-1} mm^{-1}), indicating that an enhanced wear resistance of the Ti-PCD has been achieved after the sintering process by Ti-coated diamond powders. For the annealed Ti-PCDs, no much variation of wear rate can be observed in the temperature range of 25 °C to 600 °C, while almost no wear loss can be detected for the specimens annealed at 700 °C to 800 °C. The sintered Ti-PCD is composed of the tiny, middle and big diamond grains, which corresponding the diameters of 0-5, 5-15, ~25 μm, respectively. It has been demonstrated in our previous work that the exfoliation of middle diamond grains mainly causes the wear loss of the annealed Ti-PCD specimens[18]. With the annealing temperature increasing from 25 °C to 600 °C, a large amount of stress-induced exfoliated tiny diamond grains grind and fluctuate between the tribological surfaces and leads to some cracks around the middle diamond grains, which results in the discontinuous exfoliated pits on the worn Ti-PCD surfaces. Some chemical conversions and oxidizations occur on the Ti-PCD surfaces at higher temperatures of 700 °C to 800 °C, which establish much rougher Ti-PCD surfaces with more middle and big diamond asperities and fewer tiny diamond grains. In this case, the middle and big diamond grains with some graphitization are difficult to be worn by Si_3N_4 balls in absence of tiny diamond grains[18]. Therefore, there is nearly no visible wear can be observed on the Ti-PCD annealed at high temperatures. As mentioned above, the excellent properties of the PCD, including the super wear resistance, were derived by the strong D-D bonds[23,30]. Therefore, the excellent wear resistance of Ti-PCD indirectly demonstrates that the D-D bonding quality of the sample has not been degraded due to the TiC barrier. In addition, a cobalt-catalytic graphitization would occur during the wear test and the annealing treatment, which might worsen the wear resistance of the annealed Ti-PCD. For the annealed Ti-PCD, the wear rate also reveals lower values than those of the annealed P-PCD with the increase of the annealing temperature. This

indicates that a great enhanced graphitization resistance of the PCD has been achieved in this work, which further confirms the results of XRD analysis.

The TiC barrier hinders the direct contact between diamond and cobalt, thus protects the diamond grains from cobalt-catalytic graphitization by cobalt and yields to an enhanced graphitization resistance of PCD. As previously mentioned, the remained metal Co phase distributed along the diamond boundaries does harm to the thermal stability of PCD, and many studies have focused on the methods to reduce its content. Typically, there are two methods were widely adopt. The one is the chemical treatment, which utilizes the strong acids to penetrate PCD for more than 10 h[15]. Another one is the electrolysis treatment, which sets the PCD as an anode to reduce the content of Co[14]. These treatments for PCD were demonstrated to facilitate to the enhancement of graphitization to some degree. However, the pores caused by the removal of Co severely damage the strength and toughness of PCD. Thanks to the application of Ti-coated diamond powders in this work, which were used as the raw material for the synthesis of Ti-PCD. The as-received TiC protection barrier, which obtained during the sintering process of Ti-coated diamond powders, can play an inhibition role in the cobalt-catalytic graphitization. Therefore, the application of Ti-coated diamond powders in this work is of great significance for the enhanced graphitization resistance and thus efficiently application of PCD to elevated temperatures.

For the PCD, a large amount of sintering holes would be produced due to the synthesis technology. Generally, the sintering holes distribute along the boundaries of diamond grain. In this case, the sintering holes provide substantial space for oxygen corrosion and become a weak region in PCD. In literatures, the oxygen corrosion of PCD, which results in a large amount of oxygen corrosion pits, always begins at the boundaries of diamond grain and gradually propagates with further oxidation, thus yields to the ruptured D-D bonds and sharply deteriorated mechanical properties of PCD[29,42,43]. Therefore, the oxygen corrosion is extremely detrimental to the wide application of PCD. For the Ti-coated diamond powders, the sintering process with high temperature and high pressure would lead to the chemical and covalent interaction at the interface and thus a formation of TiC phase. Hence, the oxygen might be the first to contact with TiC and produce TiO_2. The XRD results for the annealed Ti-PCD demonstrate the appearance of TiO_2 at 700 °C, while the oxidation of diamond occurs at 750 °C. This suggests that the oxidation of TiC occurs prior to that of the diamond. In this case, the TiC acts as a protective barrier to delay the oxidation of diamond in the Ti-PCD. In another words, the TiC can protect the diamond against early oxidation due to the initial formation of a TiO_2 barrier. In summary, the Ti coating on diamond powders contributes to the enhancement of the PCD oxidation resistance through the formation of a TiC oxygen barrier.

5. Conclusions

(1) The oxidation and graphitization resistances of PCD were improved via sintering with the Ti-coated diamond powders, which were deposited by the magnetron sputtering and formed a uniform TiC protective

barrier in PCD.

(2) The as-received TiC phase acts as an effective inhibitor. The inhibitor does not inhibit the oxidation and graphitization of PCD, but it delays them, elevating the initial temperatures by ~50 ℃ and ~100 ℃, respectively.

(3) The oxidation of the TiC occurs prior to that of the diamond grains, which postpones the oxidation of PCD. Moreover, the TiC barrier could also protect diamond grains from direct contact with cobalt, thus a lower cobalt-catalytic graphitization occurs, and yields to an enhanced graphitization resistance of PCD.

Acknowledgments

This work was financially supported by the National Natural Science Foundation of China (Nos. 51875537, 41572359 and 51375466), the Beijing Natural Science Foundation (No. 3172026), the Beijing Nova program (No. Z171100001117059), the Fundamental Research Funds for the Central University (No. 2652018094) and the Natural Science Foundation of Ningxia Province (No. 2018AAC03200).

References

[1] R.H. Wentorf, R.C. Devries, F.P. Bundy, Science 208 (1980) 873-880.

[2] R.H. Wentorf, J. Phys. Chem. 12 (1971) 1833-1837.

[3] S. Dub, P. Lytvyn, V. Strelchuk, A. Nikolenko, Y. Stubrov, I. Petrusha, T. Taniguchi, S. Ivakhnenko, Crystals 7 (2017) 369.

[4] Z.S. Zhao, B. Xu, Y.J. Tian, Annu. Rev. Mater. Res. 46 (2016) 383-406.

[5] W.B. Qin, Y.Y. Liu, W. Yue, C.B. Wang, G.Z. Ma, H.D Wang, Tribol. Lett. 67 (2019) 1-9.

[6] H.P. Bovenkerk, F.P. Bundy, H.T. Hall, H.M. Strong, R.H. Wentorf, Nature 184 (1959) 1094-1098.

[7] X.L. Ma, L.P. Shi, X.D. He, L. Li, G.J. Cao, C.Y. Hou, J.C. Li, L. Chang, L. Yang, Y.S. Zhong, Carbon 133 (2018) 69-76.

[8] B. Carlo, S. Osswald, Carbon 132 (2018) 616-622.

[9] S.A. Linnik, A.V. Gaydaychuk, V.V. Okhotnikov, Surf. Coat. Technol. 334 (2018) 227-232.

[10] Y.G. Gogotsi, A. Kailer, K.G. Nickel, Nature 401(1999) 663-664.

[11] C.L. Liu, Z.L. Kou, D.W. He, Y. Chen, Int. J. Refract. Met. Hard Mater. 31 (2012) 187-191.

[12] X.H. Sha, W. Yue, W.B. Qin, C.B. Wang, Int. J. Refract. Met. Hard Mater. 80 (2019) 85-96.

[13] Y.Y. Liu, W. Yue, W.B. Qin, C.B. Wang, Carbon 124 (2017) 651-661.

[14] N.I. Polushin, M.S. Ovchinnikova, M.N. Sorokin, Russ. J. Non-Ferrous Met. 59 (2018) 557-562.

[15] J.T. Gu, K. Huang, Diam. Relat. Mater. 66 (2016) 98-101.

[16] A.S. Osipov, P. Klimczyk, S. Cygan, Y.A. Melniychuk, I.A. Petrusha, L. Jaworska, A.I. Bykov, J. Eur. Ceram. Soc. 37 (2017) 2553-2558.

[17] J. Qian, C. Pantea, J. Huang, T.W. Zerda, Y. Zhao, Carbon 42 (2004) 2691-2697.

[18] J.S. Li, W. Yue, W.B. Qin, C.B. Wang, Carbon 116 (2017) 103-112.

[19] W.S. Yang, G.Q. Chen, P.P. Wang, J. Qiao, F.J. Hu, S.F. Liu, Q.Zhang, M. Hussain, R.H. Dong, G.H. Wu, J. Alloys Compd. 726 (2017) 623-631.

[20] V.M. Chagas, M.P. Peçanha, R.S. Guimarães, A.A.A. Santos, M.G. Azevedo, M. Filgueira, J. Alloys Compd. 791 (2019) 438-444.

[21] G.H. Meng, B.Y. Zhang, H Liu, G.J. Yang, T. Xu, C.X. Li, C.J. Li, Surf. Coat. Technol. 347 (2018) 54-65.

[22] S.Q. Liu, L. Han, Y.T. Zou, P.W. Zhu, B.C. Liu, J. Mater. Sci. Technol. 33 (2017) 1386-1391.

[23] Y.H. Sun, Q.N. Meng, M. Qian, B.C. Liu, K. Gao, Y.L. Ma, M. Wen, W.T. Zheng, Sci. Rep. 6 (2016) 20198.

[24] J.H. Wu, H.L. Zhang, Y. Zhang, J.W. Li, Mater. Sci. Eng. A 565 (2013) 33-37.

[25] Z.S. Zuo, B.N. Hu, H. Chen, Q.Z. Dong, G. Yu, J. Mater. Sci. Technol. 33 (2017) 1409-1415.

[26] D.Z. Meng, G. Yan, W. Yue, F. Lin, C.B. Wang, J. Eur. Ceram. Soc. 38 (2018) 4338-4345.

[27] G.R. Li, L.S. Wang, G.J. Yang, Mater. Des. 167 (2019) 107647.

[28] Q.Q. Tian, N. Huang, B. Yang, H. Zhuang, C. Wang, Z.F. Zhai, J.H. Li, X.Y. Jia, L.S. Liu, X. Jiang, J. Mater. Sci. Technol. 10 (2017) 33-42.

[29] J.S. Li, W. Yue, C.B. Wang, Int. J. Refract. Met. Hard Mater. 54 (2016) 138-147.

[30] L. Jaworska, M. Szutkowska, P. Klimczyk, M. Sitarz, M. Bucko, R. Pawel, F. Pawel, J. Lojewska, Int. J. Refract. Met. Hard Mater. 45 (2014) 109-116.

[31] B. Yang, J.K. Yu, C. Chen, Trans. Nonferrous Met. Soc. China 19 (2009) 1167-1173.

[32] D. Berman, A. Erdemir, A.V. Sumant, Mater. Today 17 (2014) 31-42.

[33] C. Tomas, I. Suarez-Martinez, N.A. Marks, Carbon 109 (2016) 681-693.

[34] D. Berman, A. Erdemir, A.V. Sumant, Carbon 59 (2013) 167-175.

[35] Z.C. Li, H.S. Jia, H.A. Ma, W. Guo, X.B. Liu, G.F. Huang, Mech. Astron. 55 (2012) 639-643.

[36] J. Kim, S. Kang, J. Alloys Compd. 528 (2012) 20-27.

[37] S.M. Hong, M. Akaishi, H. Kanda, T. Osawa, S. Yamaoka, J. Mater. Sci. 2311 (1988) 3821-3826.

[38] M. Yahiaoui, L. Gerbaud, J.Y. Paris, J. Denape, A. Dourfaye, Wear 298-299 (2013) 32-41.

[39] M. Akhaishi, H. Kanda, Y. Sato, N. Setaka, T. Ohsawa, O. Fukunaga, J. Mater. Sci. 17 (1982) 193-198.

[40] D. Lowe, G. Machin, Metrologia 493 (2012) 189-199.

[41] R.A. Howe, J.E. Enderby, J. Phys. F: Met. Phys. 31 (1973) 12-14.

[42] T.A. Scott, Adv. Appl. Ceram. 2 (2017) 161-176.

[42] J.Y. Xu, E.M. Mansori, Wear 376-377 (2017) 91-106.

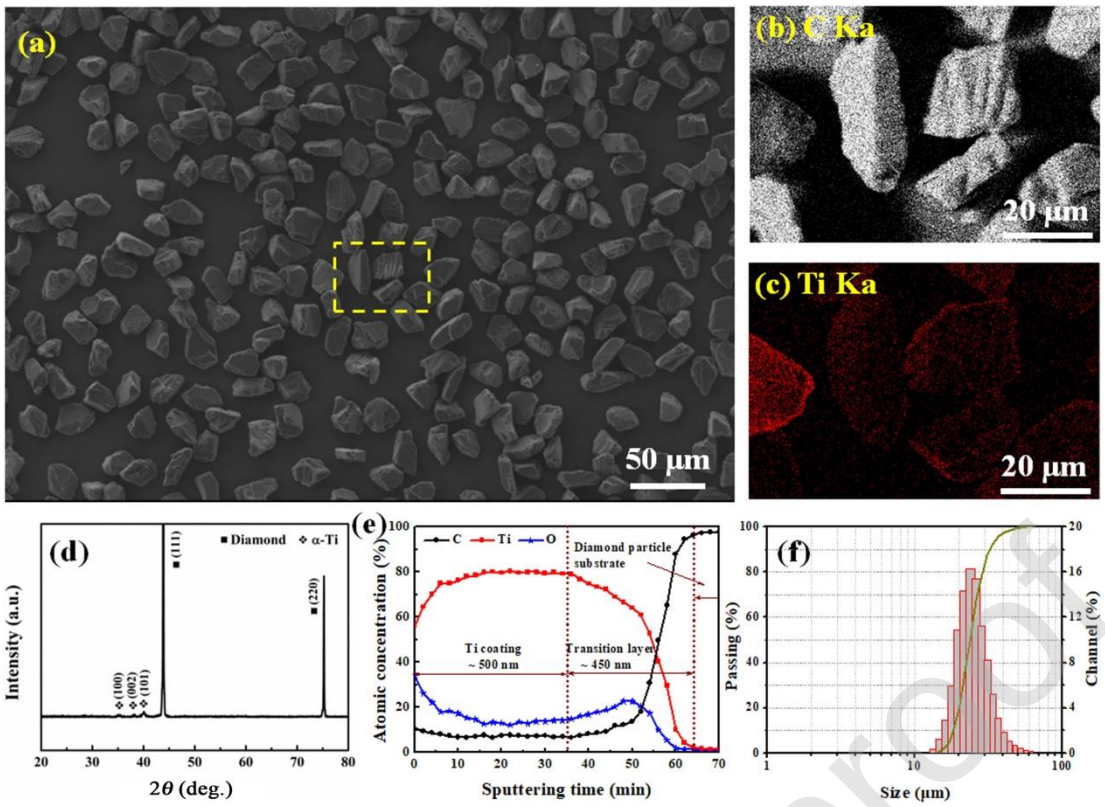

Fig. 1. Typical characteristics of the Ti-coated diamond powders: (a) SEM image of the Ti-coated diamond powders; (b, c) the corresponding EDS maps marked in the yellow detecting position of (a); (d) the XRD pattern of the Ti-coated diamond powders; (e) AES elemental depth profile of the Ti-coated diamond powders (sputtering rate: 15 nm/min); (f) particle size distribution of the Ti-coated diamond powders (D_{50}=23.75 μm).

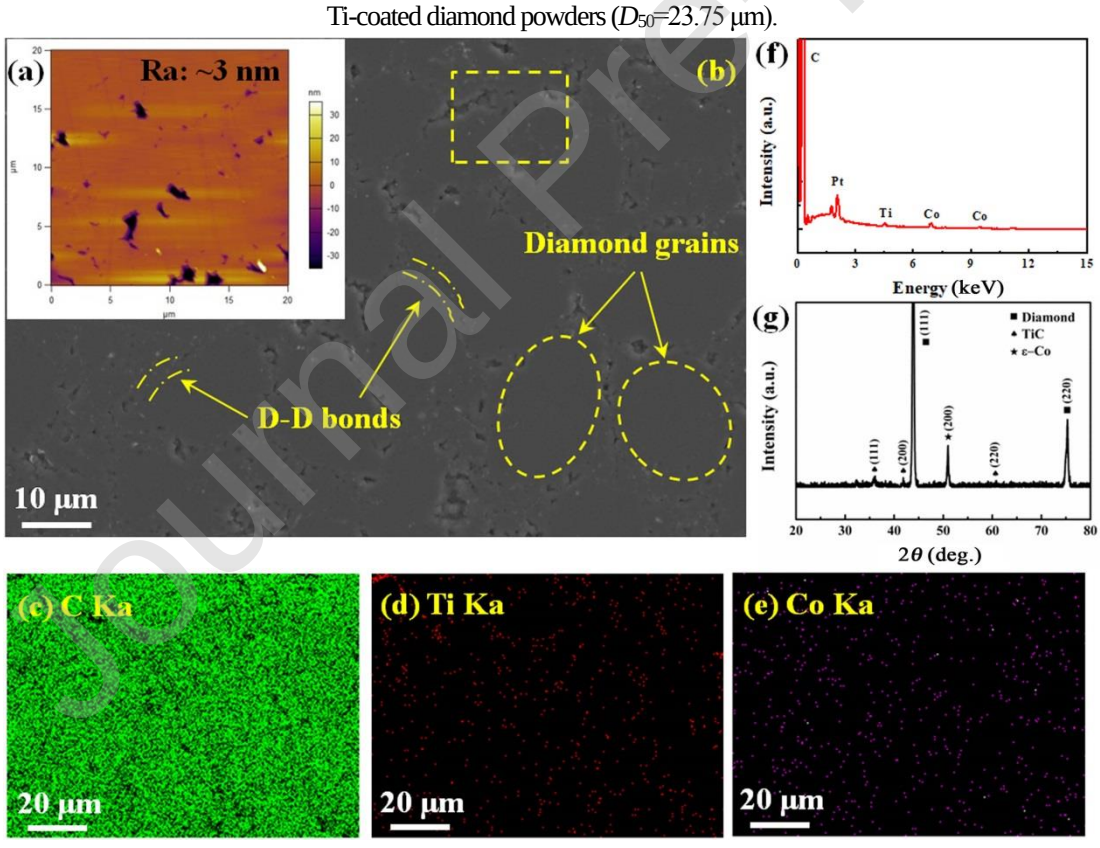

Fig. 2. Characteristics of the Ti-PCD: (a) AFM photography of the Ti-PCD surface; (b) SEM image of the Ti-PCD; (c-e) the corresponding EDS maps of (b); (f) EDS surface chemical composition marked in the yellow detecting position of (b) and (g) XRD pattern of the Ti-PCD.

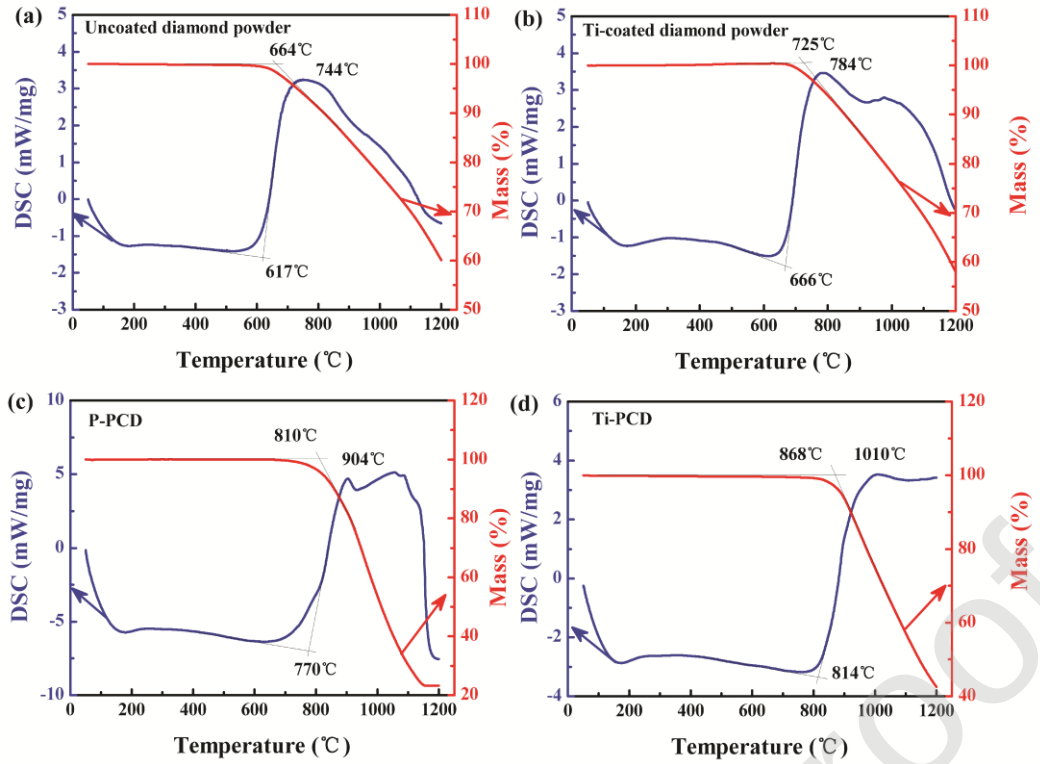

Fig. 3. DSC and TG curves of (a) the uncoated diamond powders, (b) the Ti-coated diamond powders, (c) the P-PCD and (d) the Ti-PCD heated under flowing air from 20 ℃ to 1200 ℃.

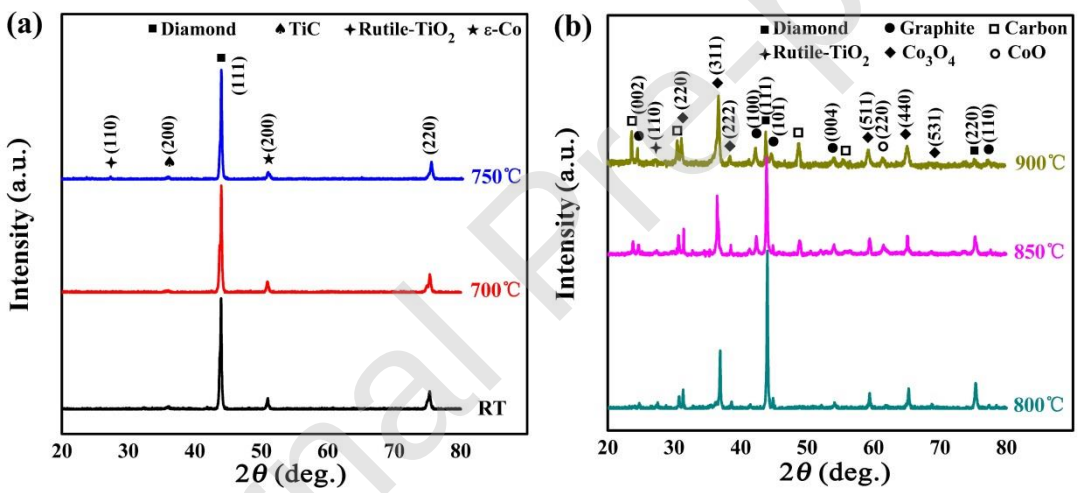

Fig. 4. XRD patterns of the Ti-PCD annealed in air: (a) RT, 700 ℃ and 750 ℃; (b) 800 ℃, 850 ℃ and 900 ℃.

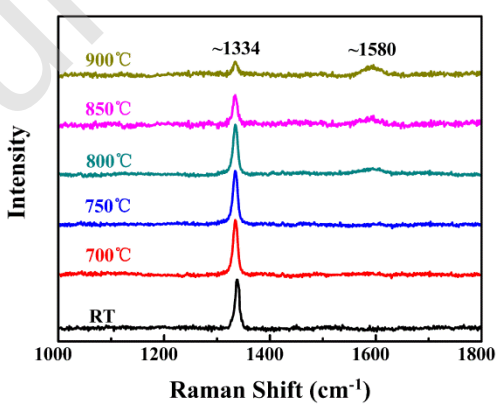

Fig. 5. Raman spectra of the Ti-PCD annealed at various temperatures under air ambient.

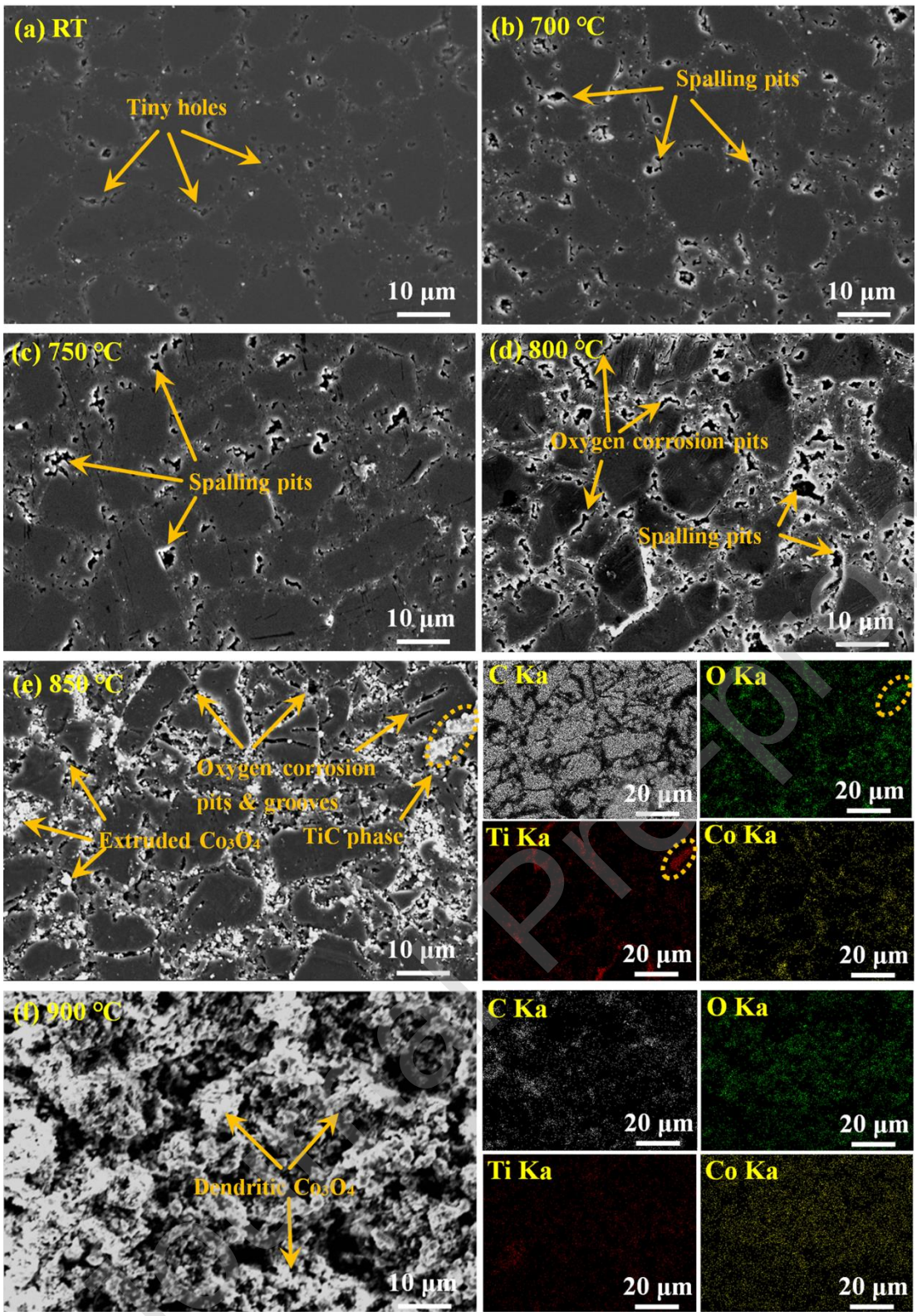

Fig. 6. Typical SEM micrographs and corresponding EDS maps of the annealed Ti-PCD surfaces in air: (a) RT; (b) 700 °C; (c) 750 °C; (d) 800 °C; (e) 850 °C; (f) 900 °C.

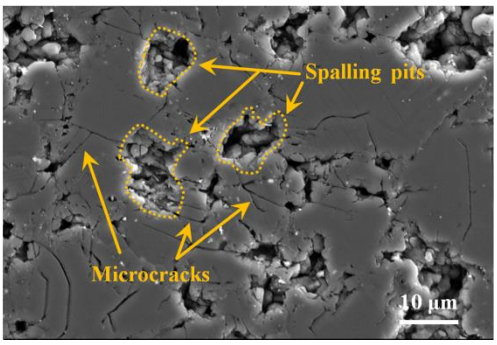

Fig. 7. Enlarged SEM image of the Ti-PCD surface annealed at 750 ℃.

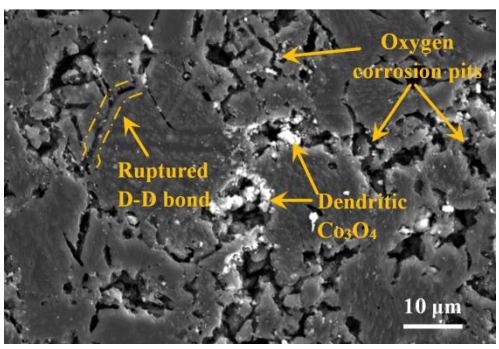

Fig. 8. Enlarged SEM image of the Ti-PCD surface annealed at 800 ℃.

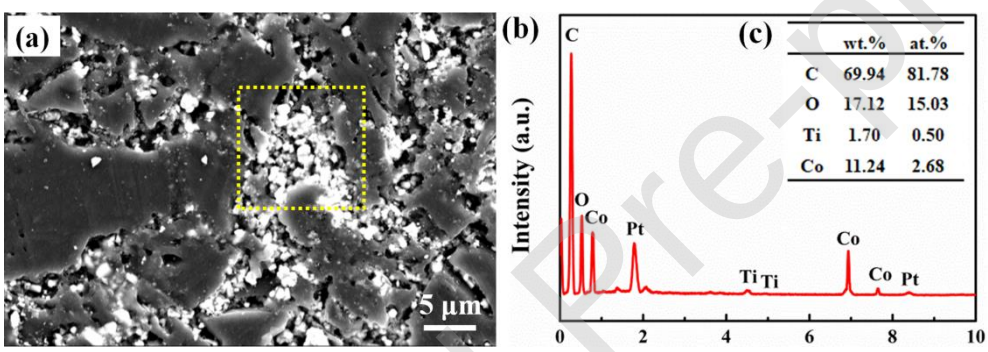

Fig. 9. SEM image and EDS of the Ti-PCD surface annealed at 850 ℃ in air: (a) the enlarged SEM image; (b, c) the EDS surface chemical composition marked in the yellow detecting position of (a).

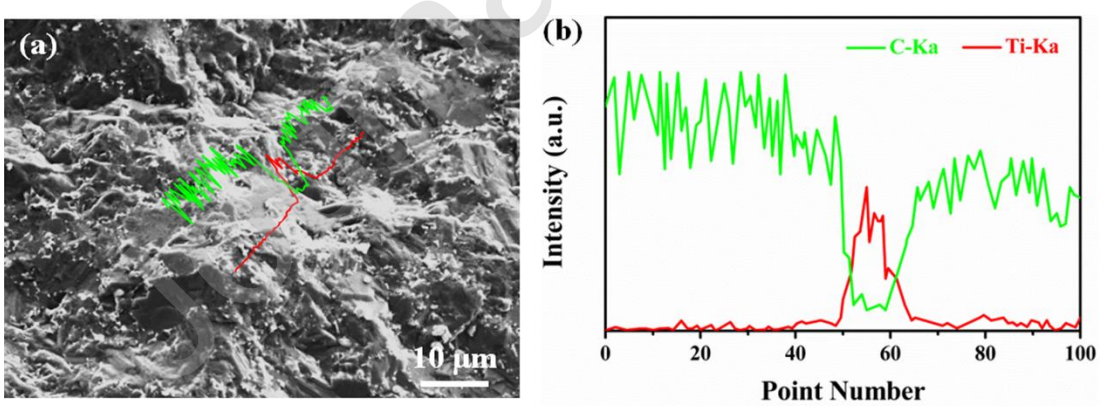

Fig. 10. EDS line scans of the cross-sectional surface of Ti-PCD.

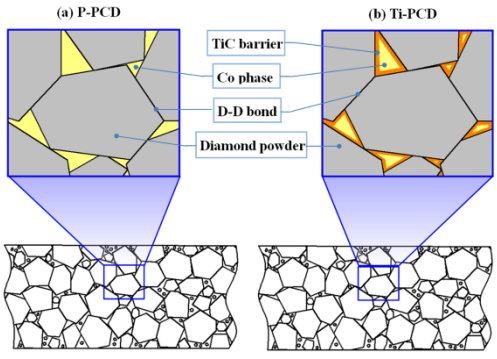

Fig. 11. Schematic diagram of the PCD structures: (a) P-PCD; (b) Ti-PCD.

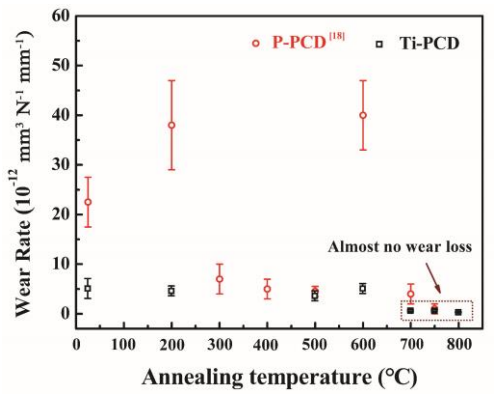

Fig. 12. Wear rates of the PCD discs annealed at different temperatures. The black scatters reveal the wear rates of Ti-PCD annealed at different temperatures, and the red scatters show those of the P-PCD[18].